Journal of Applied Phycology (2025) 37:3939–3953
https://doi.org/10.1007/s10811-025-03690-y

RESEARCH

Investigation of marennine quality throughout the main culture phases of *Haslea ostrearia* in a membrane photobioreactor

Elodie Pedron[1,2] · Jean-Luc Mouget[3] · Marylise Duperthuy[4] · Annabelle Mathieu-Denoncourt[4] · Céline Laroche[5] · Réjean Tremblay[2] · Jean-Sébastien Deschênes[6] · Olivier Gonçalves[1] · Anthony Massé[1]

Received: 11 April 2025 / Revised: 16 September 2025 / Accepted: 24 September 2025 / Published online: 10 November 2025

Abstract

Marennine is a blue pigment excreted by the diatom *Haslea ostrearia*. This pigment is renowned for its antioxidant and antibacterial properties, which have raised research interest. The standard method for obtaining marennine is by harvesting the supernatant from cultures of *H. ostrearia* and applying a double ultrafiltration approach. Marennine concentration is then assessed by another standard method (UV-visible spectrophotometry). The resulting "blue water" may however contain marennine along with a variety of other molecules, not detectable by spectrophotometry. As changes in supernatant composition are likely to occur depending on culture conditions and modes of operation, it is wondered whether this affects the marennine extract's quality. This work aims to assess such fluctuations across the exponential, stationary, and senescent phases of a *H. ostrearia* culture in a membrane photobioreactor (MPBR). Antioxidant and antibacterial bioassays, in conjunction with spectral analyses of marennine extracts, were used to characterize them. Results showed that marennine production peaked during exponential growth phase of the culture and that the resulting extract exhibited the highest antibacterial activity. Antioxidant activity was however unaffected throughout the different growth phases, being solely a function of the marennine concentration as assessed by the standard measurement approach.

Keywords *Haslea ostrearia* · Pigments · Marennine · Bioactivities · Quality indicators · Production conditions

Introduction

Marennine is a water-soluble blue pigment synthesized by the pennate diatom *Haslea ostrearia*. Latest studies on its structure (Pouvreau et al. 2006a; Gastineau et al. 2014; Yusuf et al. 2023; Zebiri et al. 2023; Bélanger et al. 2025) have concluded that marennine is a sulfated heteropolysaccharide that exists in two forms: intracellular (IMn) and extracellular marennine (EMn). Both forms exhibit a polydisperse nature, with a mean molecular weight of approximately 10 kDa. The origin of marennine's blue color remains undetermined, but a polyphenolic chromophore is considered the most plausible hypothesis (Pouvreau et al. 2006a; Gastineau et al. 2014).

Research interest in marennine has been driven by its numerous biological properties, antioxidant and antibacterial properties among others (Bergé et al. 1999; Pouvreau et al. 2008; Tardy-Laporte et al. 2013; Gastineau et al. 2014; Turcotte et al. 2016; Falaise et al. 2019a, 2019b; Permatasari et al. 2019; Bouhlel et al. 2021; Prasetiya et al. 2021; Bachtiar et al. 2024). The diverse range of bioactivities presents

✉ Elodie Pedron
pedronelodie@gmail.com

1 UMR CNRS 6144, GEPEA, 37 Boulevard de l'Université, 44602 Saint-Nazaire Cedex, France

2 Institut des sciences de la mer de Rimouski, Université du Québec à Rimouski, 310, allée des Ursulines, C.P. 3300, Rimouski, Québec G5L 3A1, Canada

3 Laboratoire Biologie des Organismes, Le Mans Université, Avenue Olivier Messiaen, 72085 Santé, Environnement, Le Mans, France

4 Département de microbiologie, infectiologie et immunologie, Faculté de médecine, Université de Montréal, Pavillon Roger-Gaudry, 2900, boulevard Édouard-Montpetit, Montréal, Québec H3T 1J4, Canada

5 Institut Pascal UMR CNRS 6602, Université Clermont Auvergne, Polytech Clermont, BP 10448, F-63000 Clermont-Ferrand, France

6 Département de mathématiques, d'informatique et de génie, Université du Québec à Rimouski, 300, Allée des Ursulines, Rimouski, Québec G5L 3A1, Canada

numerous opportunities for valorization. Several applications have already been investigated, particularly in the fields of aquaculture, cosmetics and medicine (Bergé et al. 1999; Turpin et al. 2001; Gastineau et al. 2014; Falaise et al. 2019a; Chehouri et al. 2025).

Establishing scalable, convenient and reliable production methods is crucial for developing further and broader practical applications for marennine. To date, research efforts have largely focused on optimizing culture conditions to enhance marennine productivity. Various approaches – open batch and fed-batch systems, closed photobioreactors (PBRs) with optimized parameters, biofilm versus suspended biomass cultivation, semi-continuous systems, and membrane PBRs – have been explored (Gastineau et al. 2014; Nghiem Xuan et al. 2021; Adjout et al. 2022; Gargouch et al. 2022; Prasetiya et al. 2022; Pedron et al. 2023). Various operation modes have proved their relevance for *H. ostrearia* cultivation, sometimes enabling to apply distinct residence times for the biomass versus the culture supernatant (Gargouch et al. 2022; Prasetiya et al. 2022). As marennine accumulation in the culture medium causes a decrease in available light for cell growth and marennine synthesis (Pouvreau et al. 2007; Prasetiya et al. 2016), decreasing the residence time of the culture supernatant allows to reduce this phenomenon and increases marennine productivity.

To achieve such decoupling, the use of submerged membranes offers a simple and cost-effective solution. These systems enable the semi-continuous removal of marennine-rich culture supernatant while maintaining the algal biomass in a perfusion cultivation mode (Rossignol et al. 2000; Gargouch et al. 2022; Pedron et al. 2023), increasing the volumetric productivity of the culture process. Compared to more complex post-culture separation methods, *in situ* submerged membrane setups combined the marennine production, harvesting and separation processes and are more easily scalable. Furthermore, the feasibility of long-term (150 days) fed batch cultures of *H. ostrearia,* has been recently demonstrated (Prasetiya et al. 2022), supporting the feasibility of long term cultivation of *H. ostrearia* and marennine production.

Yet, in any production system, the culture supernatant composition may evolve over time, inducing shifts in cultivated microorganism physiology (Myklestad et al. 1989; Martinho De Brito et al. 2023). Diatoms, including *H. ostrearia*, produce extracellular polymeric substances (EPS), whose composition, structure and productivity vary with physiological state and environmental factors like irradiance, temperature, and nutrient availability (De Brouwer and Stal 2002; Underwood et al. 2004; Shnyukova and Zolotariova 2015; Laroche 2022). Consequently, the production of EPS – including extracellular marennine (EMn) – might be influenced by these variables, and the resulting heterogeneity might pose challenges for ensuring consistent extract quality.

The standard method to produce EMn extract is a two-step ultrafiltration process (Pouvreau et al. 2006b), which yields a partially refined but not purified solution. Consequently, differences in culture conditions and harvest timing, which affect the composition of the supernatant, can directly impact the consistency and functionality of the resulting EMn extracts. Moreover, these variations may not be detectable through the standard method of assessing EMn extract, which typically involves UV-Visible spectrophotometry.

The present work aims to study whether variations in marennine extracts occur throughout the exponential, stationary and senescence phases of a *H. ostrearia* culture in a MPBR, and whether this impacts their quality. For practical purposes, the "quality" of marennine extract will be assessed by its level of antibacterial and antioxidant activities. Complementary analyses through fluorimetry, pigment composition as well as UV-Visible and infrared spectroscopy will also be used to further interpret the results. The study's findings will contribute to further optimize the production process by identifying the culture conditions that yield a consistent quality EMn extract, thereby facilitating its potential valorization.

Material and methods

Microalgae and culture maintenance

Haslea ostrearia NCC531 was provided by the Nantes Culture Collection (NCC, Nantes University, France). This strain was isolated from Bourgneuf Bay (Loire-Atlantique, France).

A modified Provasoli medium based on natural seawater was used for strain maintenance. After being collected, seawater was filtered through a 0.2 µm pore diameter capsule (Sartobran P) and stored in the dark. Before use, the seawater was autoclaved and enriched according to Provasoli ES 1/3 (Provasoli et al. 1957). The salinity of the solution was adjusted to 28 ppt with nanopure water and the pH to 7.8 using 5 M HCl solution. The medium was then sterilized using a 0.2 µm cut-off filtration unit (Sartolab P20 Plus).

The strains were maintained in 500-mL Erlenmeyer flasks filled with 250 mL of culture, placed at 16 °C, and illuminated by white LEDs at 100 µmol photons m^{-2} s^{-1}, following a 14/10 h light/dark cycle. The cultures were subcultured every 2 weeks, without being stirred in between. One month prior to transfer into the MPBR, cells were acclimated to the same light conditions and maintained in exponential growth to minimize stress-related variability and ensure a smooth transition to photobioreactor cultivation. To do so, cells were subcultured every 4 days at 18 °C, to maintain the exponential growth phase and illuminated using white LEDs at 200 µmol photons m^{-2} s^{-1}, following a 14/10 h light/dark cycle. Cultures were manually stirred once a day, at the beginning of the light cycle.

Membrane photobioreactor system setting

The hollow-fiber membrane photobioreactor (MPBR) proposed by Gargouch et al. (2022) was used (Fig. 1). It is composed of two main elements: a 1 L airlift-type culture chamber (vertical flat panel) and a hollow-fiber membrane submerged inside the culture.

The algal culture was placed in an air-conditioned room with a temperature adjusted to 18°C. Light was provided by a white LED panel placed in front of the MPBR, with the distance calibrated to deliver an irradiance of 200 µmol photons m^{-2} s^{-1}, and a 14/10h light/dark cycle was applied. The pH was fixed at 7.8 and was maintained via CO_2 injection into the culture chamber, which was regulated by an automated valve. Setpoints were maintained using a homemade LabView interface. Light and temperature parameters were selected to promote both optimal growth conditions for *H. ostrearia* and production of marennine.

The membrane was composed of polyvinylidene fluoride (PVDF) hollow fibers (VMA Industries, France), one end of which was closed. The pore diameter was 0.05 µm with a total surface area of 0.04 m^2 (Gargouch et al. 2022).Using a peristaltic pump, 100 mL of culture supernatant was harvested daily via filtration and replaced with 100 mL of fresh culture medium. The dilution rate (D, day^{-1}) was fixed at 0.1 day^{-1} and calculated as follows:

$$D = \frac{Q}{V_r} \quad (1)$$

with Q the permeate suction rate (mL day^{-1}), and V_r the total volume of culture in the reactor (mL).

The residence time of biomass tended toward infinity as it was entirely retained in the reactor by the membranes (excepted for sampling), and the culture volume was maintained constant as semi-continuous filtration of the culture was compensated by the addition of fresh nutritional medium. The MPBR's perfusion mode enabled the separation of the residence time of EMn in the supernatant from that of *H. ostrearia* biomass, thereby allowing for the study of EMn extract evolution throughout a culture.

The culture medium was based on the Provasoli ES 1/3 recipe, enriched in nitrate, with a final concentration of $NaNO_3$ equal to 0.15 g L^{-1}. Bicarbonate and silica solutions were directly added in the culture chamber every day to reach concentrations of $NaHCO_3$ equal to 0.42 g L^{-1} and $Na_2SiO_3.5H_2O$ equal to 0.03 g L^{-1}, following a fed-batch strategy as proposed by Nghiem-Xuan (2019) to avoid salt precipitation. Briefly, after adding 100 mL of culture medium enriched in $NaNO_3$, 2mL of solution of $Na_2SiO_3.5H_2O$ at 15 g L^{-1}, and 5 mL of solution of $NaHCO_3$ at 0.84 g L^{-1} were added daily and directly to the culture.

Culture medium monitoring

The culture medium composition was monitored throughout the different MPBR culture phases. Nitrate (NO^{3-}), phosphate (PO_4^{2-}), and silicate (SiO_4^{4-}) are the main limiting ions for *H. ostrearia* cultivation (Turpin et al. 1999). Ion chromatography analysis was used to measure nitrate levels in the harvested culture supernatant. As the salinity of the medium was high (28 ppt), a 20-fold dilution was performed prior to analysis to avoid saturating the column with chloride ions. The ICS 900 anion chromatography system (Dionex, USA) is equipped with an AG9-HS pre-column (Dionex) and an AS9-HS column (5x250 mm) (Dionex) grafted with alkyl groups having a quaternary ammonium at the end of the chain. The eluents consisted of a 6 mmol L^{-1} Na_2CO_3 solution and a 1 mmol L^{-1} $NaHCO_3$ solution flowing at 0.9 mL min^{-1}. In addition,

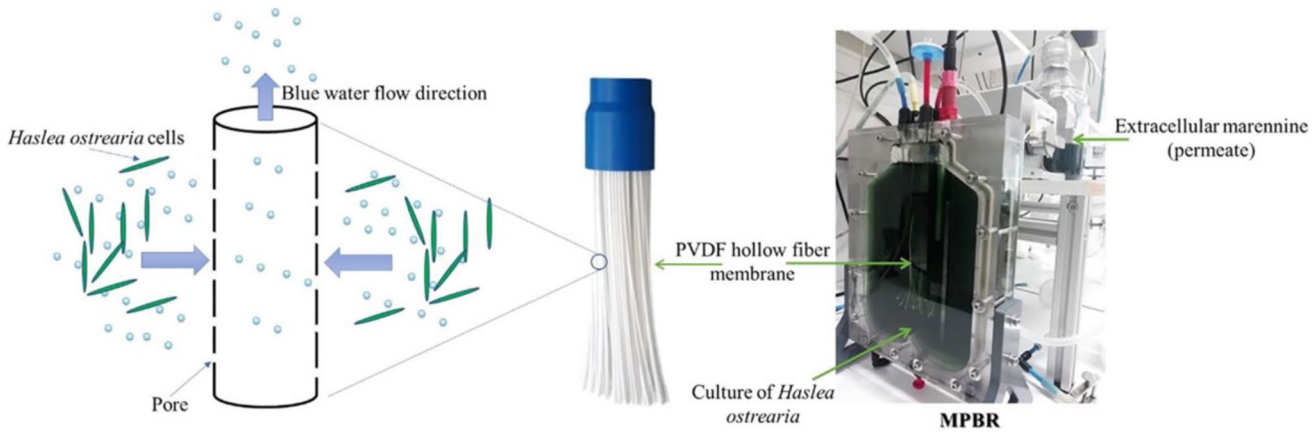

Fig. 1 Hollow-fiber membrane photobioreactor (MPBR) used for the culture of *Haslea ostrearia.* (Figure reproduced from Gargouch et al. (2022))

an AS40 automatic sample changer (Dionex) and an MMS 300 micro-membrane suppressor (Dionex) fed with a 25 mmol L^{-1} H_2SO_4 solution at a flow rate of 1.8 mL min^{-1} were used. Conductimetry was used to detect anions and cations during elution, and their concentrations were obtained using external calibration. The silicate and phosphate ions were not quantifiable by anion chromatography due to dilution. Therefore, elemental analysis was carried out by a subcontractor (QARBONE, Groupe 6NAPSE). Silicon and phosphorus were quantified using inductively coupled plasma atomic emission spectrometry (ICP-AES) (iCAP Pro Duo – Thermo Scientific).

Marennine production monitoring

The extracellular marennine (EMn) concentration in solution was determined using the spectrophotometric method proposed by Pouvreau (2006). The absorbance of the solution was measured at 669 nm using a JASCO V-630 spectrophotometer, and the concentration of EMn (mg L^{-1}) determined according to the Beer-Lambert formula:

$$[EMn] = \frac{A}{\varepsilon * l} * M \quad (2)$$

with A the absorbance measurement at 669 nm, ε the molar extinction coefficient of EMn determined by Pouvreau (2006) ($\varepsilon = 12 \times 10^4$ L mol^{-1} cm^{-1}), l the length of the optical path in the cell (cm), and M the molar mass of EMn (M = 9893 g mol^{-1}, as provided by Pouvreau (2006). Each absorbance measurement was performed in triplicate.

Volumetric EMn productivity (P_v, mg L^{-1} day^{-1}) was calculated according to the formula of Gargouch et al. (2022) :

$$P_v = [EMn] * D \quad (3)$$

with *[EMn]* the EMn concentration inside the culture chamber (mg L^{-1}), D the dilution rate applied to the culture (day^{-1}).

The production rate of EMn within the culture (R_{EMn}, mg day^{-1}) was calculated to estimate the daily quantity of marennine *de novo* accumulated inside the supernatant and used to estimate the daily EMn specific production rate of the biomass (R_{cell}, mg 10^6 $cells^{-1}$ day^{-1}):

$$R_{EMn} = \frac{([EMn]_n - [EMn]_{n-1}) * V_r + [EMn]_{n-1} * Q * \Delta t}{\Delta t} \quad (4)$$

$$R_{cell} = \frac{R_{EMn}}{(N_{n-1} + N_n)/2 * V_r} \quad (5)$$

with $[EMn]_n$ the EMn concentration inside the culture chamber at day n (mg L^{-1}), V_r the total volume of culture in the reactor (mL), Q the permeate suction rate (mL day^{-1}), and Δt, the time difference between the two sampling of supernatant (days).

The cumulative production of EMn (Pc, mg) was calculated to estimate the raw MPBR EMn production on day n using the following equation:

$$P_c = \frac{Pc_{n-1} + [EMn]_n * Q * \Delta t}{V_r} \quad (6)$$

with $[EMn]_n$ the EMn concentration inside the culture chamber at day n (mg L^{-1}), V_r the total volume of culture in the reactor (mL), Q the permeate suction rate (mL day^{-1}), and Δt, the time difference between the two sampling of supernatant (days).

Refining of culture supernatants

The culture supernatants corresponding to the permeate collected through daily filtration during MPBR cultures were filtered using a 0.2 µm cut-off filtration unit (Sartolab P20 Plus) before being stored at 4 °C and in the dark. Supernatant of culture was harvested over the 34 days of culture and the samples were separated in three lots. The first lot corresponded to the pool of samples harvested from day 4 to day 14 (BW1). The second lot was harvested from day 15 to day 26 (BW2). Finally, the last lot corresponded to the culture supernatant harvested from day 27 until the end of the culture on day 34 (BW3).

They were then pre-concentrated by ultrafiltration at a cutoff of 3 kDa (P = 22 psi), until a volume reduction factor of 10. The retention rate of marennine was calculated from the chromophore absorptivity in the initial extract and the concentrated extract. The resulting extracts (retentate) were stored at −20°C in the dark. Further refining was performed according to the double ultrafiltration approach proposed by Pouvreau et al. (2006b), as it remains to date the most cost efficient way to obtain bioactive marennine extracts in the form of a « blue water » (BW) (Falaise et al. 2019b). Diafiltration and further concentration were conducted on a 1kDa cutoff membrane up to 5 diafiltration volumes, using nanopure water (P = 50 psi) until salinity reached 0 ppt. The desalted retentates were ultrafiltrated on a 30-kDa cutoff membrane (P = 50 psi). Approximately 50 mL of each BW were obtained, thus corresponding to the intermediate fraction of the initial culture supernatant (30-3 kDa), and the samples were stored at 4 °C in the dark until further analysis. For the antioxidant activity bioassay, 15 mL of BW was freeze-dried and solubilized in 1 mL of nanopure water to increase the concentration of the tested samples.

All ultrafiltration and diafiltration steps were performed, at 20 °C, in AMICON 400mL stirred cells connected to a nitrogen flow and using Ultracel membranes.

Biomass monitoring

Daily, an hour after the beginning of the light cycle, two samples of the culture were collected. A 7 mL sample of culture was first collected and a complete mechanical homogenization was conducted using a magnetic bar in the reactor to ensure the uniformity of the culture and to resuspend any settled biomass. Then, a second 7-mL sample was collected. The sample obtained before homogenization corresponds to the fraction of cells in suspension and is referred to as the pelagic sample, whereas the sample obtained after complete homogenisation of the culture corresponds to the total biomass sample. This approach allowed us to consider the natural tychopelagic behaviour of *H. ostrearia* and its tendency to sink down in a culture.

H. ostrearia biomass growth modelling

Biomass was monitored by cell density estimation and chlorophyll *a* concentration. The cell density N (cells L^{-1}) of the culture was determined by the Nageotte cell count (Marienfeld, AQRA, India) as follows:

$$N = \frac{n}{V} \tag{7}$$

with *n* the number of cells, and *V* is the volume of sample used for counting, knowing that one strip corresponds to a volume of 1.25 µL. All counts were performed in triplicate with 300 ± 50 cells, at three random locations in the counting chamber.

Chlorophyll *a* concentration ($[Chl_a]$ (µg mL^{-1})) was used as a second biomass indicator and obtained following pigment extraction from both pelagic and total biomass sampling (detailed extraction method below).

The Gompertz model was used to fit daily cell density chlorophyll *a* data to obtain growth parameters of the culture using R software R-4.3.

$$Y = A * e^{(-e^{(-\mu_{max}*(X-X_c))})} \tag{8}$$

with *Y*, biomass concentration depending on the biomass indicator used (N 10^6 cells L^{-1} or $[Chl_a]$ ng mL^{-1}), *A*, maximum biomass concentration reached (N_{max} 10^6 cells L^{-1} or $[Chl_a]_{max}$ ng mL^{-1}), μ_{max} maximal growth rate (day^{-1}), X_c, midpoint of the exponential growth phase (day), and *X*, day of culture (day). Data were transformed using natural logarithms, and the initial biomass was calculated on day 1 (X = 1 day), considering an initial cell concentration of N = 100×10^6 cells L^{-1}, equivalent to a chlorophyll *a* concentration of $[Chl_a]$= 244 ng mL^{-1}.

Pigment analysis

Pigment composition and quantification of biomass were performed according to Ritchie (2008). Briefly, 1.5 mL of sample was centrifuged at 12,000 ×*g* for 15 min. The resulting pellets were resuspended in 1.5 mL of 90% acetone then homogenized by sonication. Samples were then placed in the dark for 3 h at 4 °C for extraction, followed by another 15 min of centrifugation at 2,400 ×*g*. The absorbances at 480, 630, 645, 665, and 750 nm were measured on resulting supernatants (JASCO V-630 spectrophotometer). Pigment concentrations were calculated according to the following equations (Strickland and Parsons 1968; Ritchie 2008):

$$[Chl_a] = (-0,3002 * (A_{630} - A_{750}) - 1,7538 * (A_{645} - A_{750}) + 11,9092 * (A_{665} - A_{750})) * \frac{V_{acetone}}{V_{sample}} * 1 \tag{9}$$

$$[CarT] = (4 * (A_{480} - A_{750})) * \frac{V_{acetone}}{V_{sample}} * 1 \tag{10}$$

$$P^{T}_{spe} = \frac{[Chl_a] + [CarT] * 10^3}{N} \tag{11}$$

with A_λ the absorbance at the given wavelength (λ), $V_{acetone}$ the volume of acetone used for pigment extraction (mL), V_{sample} the volume of sample (mL), *l* the length of the optical path (cm), $[Chl_a]$ and *[CarT]* respectively, chlorophyll *a* (µg mL^{-1}), total carotenoids concentration (µg mL^{-1}), *N* the cell density of the culture (cells L^{-1}), and P^{T}_{spe} the total specific pigment content (µg (10^6 cells)$^{-1}$).

Photosynthetic parameters monitoring

From the pelagic daily sample, 2 mL of culture were used for photosynthetic parameter estimation using a Water-PAM fluorometer (cuvette version, Walz GmbH, Germany) as complementary indicator on the physiological state of the cells found in suspension in the culture (Consalvey et al. 2005). This aims to provide an indication of the photosynthetic state of the cells by analyzing the suspended biomass that was exposed to light at the time of the daily sampling. The sample was first dark-adapted for 15 min and then introduced into a 10-mm quartz glass cuvette of the PAM fluorometer, which was controlled using WinControl-3 software. The maximum PSII quantum efficiency (F_v/F_m) was measured using a 600-ms saturating pulse (2500 µmol photons m^{-2} s^{-1}):

$$\frac{F_v}{F_m} = \frac{F_m - F_0}{F_m} \tag{12}$$

with F_0, the minimum fluorescence yield of dark-adapted cells, F_m, the maximum fluorescence yield of dark-adapted cells during the saturating flash, and F_v (= F_m - F_0), the variable fluorescence.

To provide detailed information on the overall photosynthetic performance of microalgae, photosynthesis/light (P/E) curves were constructed using nine 30-s incremental irradiance steps (0, 75, 109, 165, 245, 346, 479, 773, 1127 µmol photons m^{-2} s^{-1}) and calculating the relative electron transport rate (rETR) through PSII for each level of actinic irradiance:

$$\frac{F_q'}{F_m'} = \frac{F_{m'} - F'}{F_m'} \tag{13}$$

$$rETR = \frac{F_q'}{F_m'} * \frac{PAR}{2} \tag{14}$$

with *PAR* the actinic irradiance (= Photosynthetic Active Radiation from 400 to 700 nm), F_q'/F_m', F_q', F', F_m' the effective quantum yield of PSII, the variable fluorescence, the fluorescence, and the maximum fluorescence intensity in the light at a given PAR intensity, respectively, and *2* the division factor based on the assumption that half of the absorbed photons are equally distributed between PSI and PSII.

The Michaelis-Menten equation was used to model the P/E curve rETR as a function of PAR, using R software R-4.3:

$$rETR = \frac{rETR_{max} * PAR}{Em + PAR} \tag{15}$$

The P/E curve enabled the estimation of the effective quantum efficiency of the culture at growth irradiance, $F_q'/F_m'_{200}$, used as a proxy for the photosynthetic state inside the culture chamber.

Bioactivity analysis

Antibacterial activity

Vibrio splendidus 4D1-8 was selected for its growth inhibition response to marennine extract (Falaise et al. 2019b). The strain was supplied by the Laboratoire de biologie intégrative des modèles marins (LBI2M) (Station biologique de Roscoff, France) and was isolated from oyster tissues; *V. splendidus* 4D1-8 showing moderate virulence against them (Oyanedel et al. 2020).

Vibrio strain was maintained at −80 ◦C in 20% glycerol. Broth cultures were prepared with autoclaved, cation-adjusted, LB broth media by the addition of 2% NaCl (LB 2% NaCl) (10 mg mL^{-1} tryptone (Termo Fisher), 5 mg mL^{-1} yeast extract (Thermo Fisher), 20 mg mL^{-1} NaCl) and strains were isolated on LB- 2% NaCl- 1.2% agar media (LBA 2% NaCl) from the −80°C. Plates containing the isolated colonies were kept at room temperature for no more than a week. Before the test, three different colonies per Petri dish (biological replicates, $n = 3$) were inoculated in 5 mL LB 2% NaCl and grown overnight at room temperature (20°C) under moderate agitation (130 rpm). The next day, 100 µL of the bacterial suspension were transferred into 5 mL of LB 2% NaCl and incubated at 20 °C with agitation until the bacterial suspension reached an optical density at 600 nm (OD_{600}) of 2. This inoculum was subcultured 2 h before the antibacterial response test to ensure that the inoculum was growing exponentially. Right before inoculation of the 96 wells microplate, 1 µL of the inoculum was subcultured in 14 mL of three times concentrated LB 2% NaCl (3xLB 2% NaCl) culture medium, to obtain an inoculum of OD_{600} of 0.0001.

Vibrio splendidus was exposed to a series of the tested extracts (dilution carried with 3xLB 2% NaCl). Antibacterial activity was evaluated in a 96-wells microplate in which 25 µL of inoculum were added to 75 µL of tested marennine extract. Each concentration was tested in technical triplicates, and a blank was prepared with 25 µL of 3xLB 2% NaCl and 75 µL of the corresponding dilution of BW. Bacteria were incubated at 20 °C with 160 rpm agitation for 24 h, after which the level of growth was assessed by measuring the absorbance at 600 nm (SpectraMax ID3 plate reader). The growth inhibition (%) of *V. splendidus* was estimated from the following equation:

$$Growthinhibition = \frac{\left(Abs_t - Abs_{LB}\right) - \left(Abs_i - Abs_{EMn}\right)}{\left(Abs_t - Abs_{LB}\right)} \tag{16}$$

with Abs_t the absorbance at 600 nm of the well containing 100 µL the *V. splendidus* strain culture, Abs_{LB} the absorbance at 600 nm of well containing 100 µL LB medium, Abs_i the absorbance at 600 nm of the well containing the *V. splendidus* exposed to a concentration of EMn extract, Abs_{EMn} the absorbance at 600 nm of the well containing non-inoculated LB culture medium and the corresponding solution of EMn extract.

Bacterial growth inhibition results were modeled as a dose-response curve following a four-parameter logarithmic function using the "drda" package and R software R-4.3. Each extract was tested three times with three different clones ($n = 3$) and the results of each test were modeled separately.

Antioxidant activity

The DPPH (2,2-diphenyl-1picrylhydrazyl) scavenging assay of EMn was performed using a Dojindo DPPH assay

kit, according to the method reported of Shimamura et al. (2014) adapted to marennine extract at all purification levels, to facilitate future comparisons. The initial DPPH solution (0.2 mM) was diluted 5-fold (0.04 mM) to make the activity detectable within our low concentration range of EMn extract ([EMn] maximum concentration reaching 2 µmol L^{-1}, dilution carried with nanopure water). As proposed by Gang et al. (2021), the 99% ethanol used to prepare the DPPH solution was replaced by 70% ethanol, which is more suitable for saline extracts. For each microplate, the antioxidant capacity of a positive control, the antioxidant Trolox ([Trolox] maximal concentration reaching 8.0 µmol L^{-1}), was also tested to ensure the reliability of the DPPH solution used.

After 20 µL of the tested sample, EMn extract or Trolox solution, 80 µL of 0.1 M Tris–HCl buffer (pH 7.4), and 100 µL of the DPPH solution (0.04 mM) were added to the microplate wells. After completing the microplate, the plate was shaken for 30 s and left at room temperature in the dark for 30 minutes, after which the absorbance of the solution at 517 nm was measured (SpectraMax 190 microplate reader). On each microplate, a mixed solution of 120 µL of ethanol and 80 µL of Tris–HCl buffer was used as the blank for the Trolox, 100 µL of ethanol and 20µL of nanopure water, and 80 µL of Tris–HCl buffer were used as the blank for the absence of EMn, and as the EMn absorbed near 517 nm, 100 µL of ethanol and 20µL of EMn extract solution at each tested concentration, and 80 µL of Tris–HCl buffer were used as the blank for BW. The absorbance at the addition of the tested sample was expressed as A_s, the absorbance at the addition of the corresponding blank as A_c, and the inhibition ratio (%) was obtained using the following equation:

$$\mathrm{DPPHinhibition} = \frac{A_c - A_s}{A_c} * 100 \quad (17)$$

Spectral analysis

A Bruker Tensor 27 spectrometer equipped with a HTSXT plate reader module, an RT- DLaTGS deuterated triglycine sulphate detector and OpusLab v 7.0.122 software (Bruker Optics, Germany) was used for the Attenuated total reflectance - Fourier-transform infrared (ATR-FTIR) spectra acquisition. Infrared spectra were recorded in transmission mode, using freeze-dried extracts deposited directly on the spectrometer objective. Spectral resolution was set at 1 cm^{-1}, with 32 scans. Absorbance spectra were collected between 4000 cm^{-1} and 400 cm^{-1}, and the aperture diameter of the microplate reader was set at 3 mm. Background spectra were collected using the same instrument settings as those used for the samples.

For UV–visible (UV–vis) spectral acquisition, a Cary 100 spectrophotometer (Agilent/Varian, USA) combined with Varian WinUV software (version 3.00) was used. UV–Vis samples were analyzed at 24 °C in quartz cuvettes.

Spectra processing was done with Spectragryph optical spectroscopy software (v1.2.16.1).

Statistical analysis

Statistical analysis was performed using the XLSTAT software. EMn specific and volumetric productivities, specific chloroplast pigment concentrations, and effective quantum yield of PSII evolution over 34 days of culture were analyzed through the mean of 5 consecutive days (comparison of 6 periods after start of growth) using one-way ANOVA. The normality of distributions and homoscedasticity of variances were tested beforehand using the Shapiro-Wilk and Levene tests. When differences were detected, Fisher's LSD multiple-comparison test were used to deduce which values were significantly different. Significance of differences was defined at $p < 0.05$. The replication unit was the number of days in each phase.

For the antibacterial bioactivity assay, the concentration of sample needed to inhibit 20% of bacterial growth (IC20) was computed by modeling growth inhibition (%) versus sample concentration for each clone tested ($n = 3$). Comparison was made based on IC_{20} instead of IC_{50} because the amount of EMn extracts available did not permit experimentally to reach 50% bacterial growth inhibition for all the three lots tested. Statistical analyses were conducted using XLSTAT. One-way ANOVA was used to analyze differences in IC_{20} according to the three BW lot tested. Significant differences at $P < 0.05$ between mean IC_{20} were determined using Fisher LSD's multiple comparison test.

For the antioxidant assay, the difference in bioactivity efficiency of the three EMn extracts tested was analyzed by a two-way ANCOVA with the harvest time and EMn concentration as comparative factors to determine the significance of the qualitative factor considering the linear dose-response relation between antioxidant activity and EMn concentration at the tested concentrations.

All statistical results are presented in supplementary materials.

Results

Culture characterisation in MPBR

Monitoring of marennine production

EMn productivities in the MPBR were variable over the 34 days of culture (Fig. 2). During the first 14 days of culture, the EMn production rate normalized to the amount of biomass (R_{cell}) was the highest, with a mean of 7.3 ± 2.6 mg 10^6 $cells^{-1}$ day^{-1} of EMn and a maximum of 12.4 ± 1.7 mg 10^6

cells^{-1} day^{-1} of EMn. Thus, the first 14 days were characterized by the accumulation of marennine in the culture medium (online resource **Fig.** S1), *H. ostrearia* cells producing more EMn than harvested with a dilution rate at 0.1 day^{-1}. This resulted in a net accumulation, which increased the EMn volumetric productivities (P_v) of the MPBR, leveling off at 2.1 ± 0.1 mg L^{-1} day^{-1} of EMn from day 15 to day 21, as R_{cell} stabilized around 3.1 ± 0.8 mg 10^6 cells^{-1} day^{-1} of EMn. The EMn concentration in the culture then reached a maximum at 21.2 ± 0.7 mg L^{-1} (online resource Fig. S1).

Thereafter a marked shift in the production pattern was observed, starting on day 22, when cells displayed a non-significant level of R_{cell} up to the end of the culture. This decrease reveals a reduction in EMn biosynthesis rather than a dilution effect, indicating either a metabolic downregulation of EMn production or an alteration in cellular physiology. Consequently, P_v steadily decreased from day 25 and no further increase in P_c, the cumulative amount of EMn harvested over time, was observed (no accumulation of EMn). Thus, after 35 days of culture, P_c reached 46.1 ± 0.4 mg of EMn (**Fig.** 2).

Cell population evolution in MPBR

Three main stages of culture were observed when following the evolution of *H. ostrearia* cell population in the MPBR using both biomass indicators, N and [Chl_a]: the exponential stage, followed by the stationary stage, and then the senescent stage (**Fig**. 3**,** online resource **Table** S1). Both biomass indicators showed an exponential growth phase from day 0 to day 14, then a stationary phase starting on the 15th day. Both biomass indicators did not display the same day-to-day variability during stationary phase, which appears steadier when monitoring [Chl_a] than N. From day 25 to the end of the culture, a regular decrease in chlorophyll *a* concentration was observed, followed by a decrease in cell concentration, with a lag of almost 10 days, marking the entrance into the senescent stage of the culture (**Fig.** 3).

The pelagic portion of the biomass leveled off around the 12th day: this population then represented approximately 1/6th of the total biomass (Fig. 3). It did not display a very constant concentration, but rather an oscillation pattern noticeable with either of the two biomass indicators, N and [Chl_a]. Afterwards, similarly to the total biomass population, the concentration of pelagic cells and their chlorophyll content began to decrease as early as day 20, meaning a lower ratio of living cells resuspended in the water column.

Physiological state monitoring

The physiological state of *H. ostrearia* cells, monitored daily *via* analysis of pigment composition, is displayed in Fig. 4 and detailed in **Table S2** (online resource). From the total biomass sample, the cell pigment content appeared stable during the exponential growth phase and the early stationary phase, with a total pigment content of 2.9 ± 0.1 and 2.7 ± 0.2 µg 10^6 cells^{-1}, respectively. The pigment content started to decrease in the late stationary phase, reaching a mean pigment content of 2.6 ± 0.1 µg 10^6

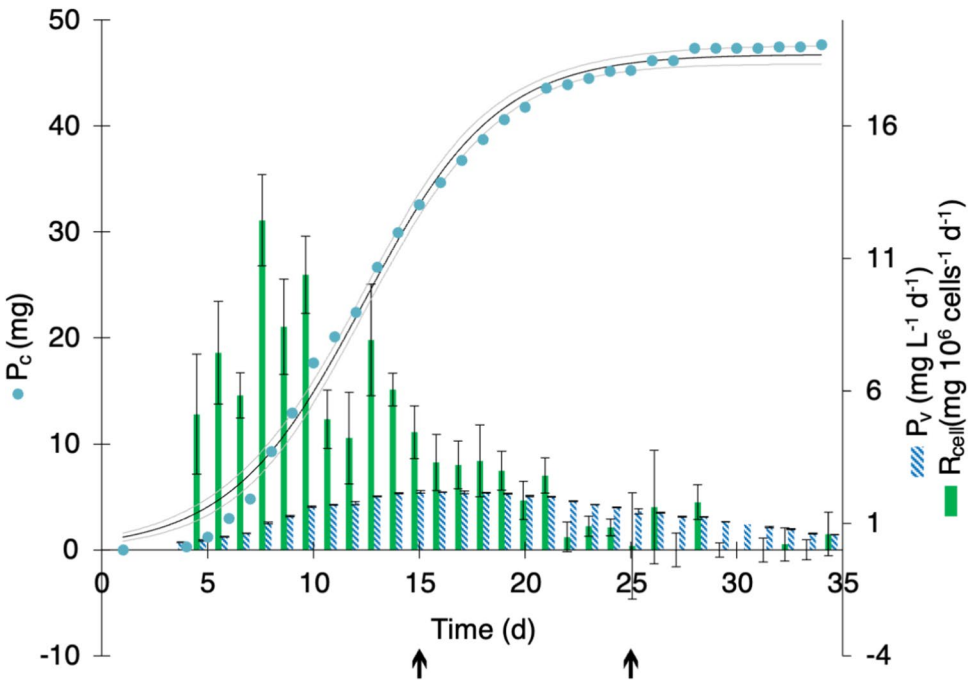

Fig. 2 Evolution of marennine production in *H. ostrearia* NCC 531 MPBR culture (D = 0.1 day^{-1}). EMn volumetric productivity P_v (mg L^{-1} day^{-1}) in lined blue bars, represented as mean ± SD (n = 3); biomass EMn specific production rate, R_{cell} (mg 10^6 cells^{-1} day^{-1}) in plain green bars represented as calculated value ± 95% uncertainty; cumulative EMn production (P_c) (mg) in blue dots represented as calculated value ± 95% uncertainty (R^2=0.99). The arrows indicate the entrance in the stationary and senescent phases, respectively.

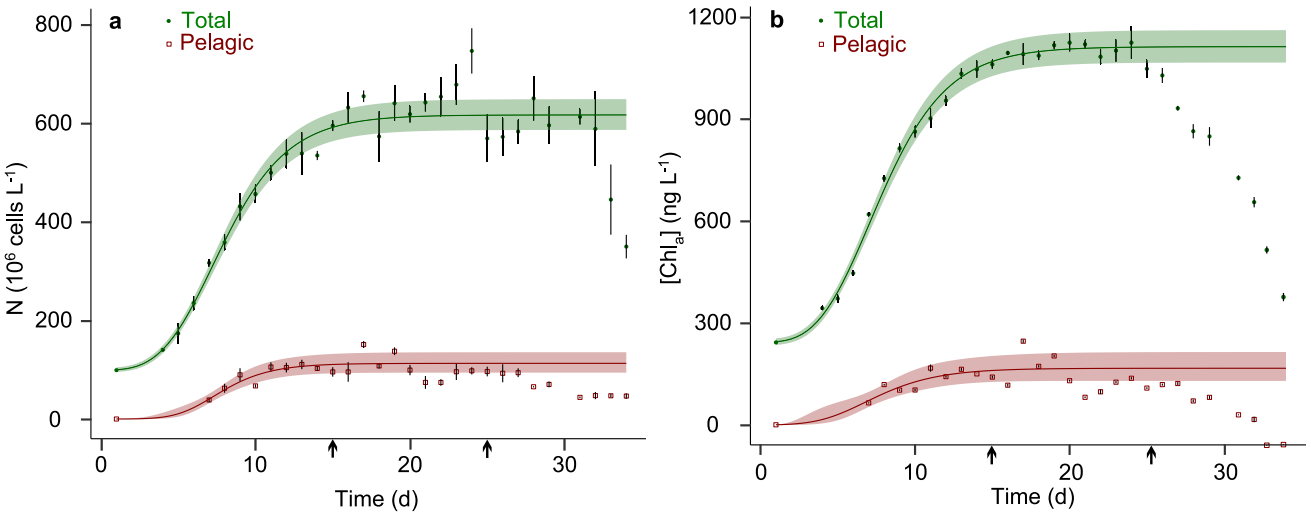

Fig. 3 Biomass growth curves measured for *H. ostrearia* NCC 531 fitting with Gompertz' model. The biomass indicators used were (**a**) cell concentration (N, 10^6 cells L^{-1}, with initial N = 100 10^6 cells L^{-1}), estimated by cell count (n = 3), as function of time (d) and (**b**) chlorophyl *a* concentration ([Chl_a], ng L^{-1}, with initial [Chl_a] = 244 ng L^{-1}), as function of time. All measurements were performed daily in triplicate (n = 3) before and after culture homogenization, to sample both pelagic (red squares, pelagic) and total biomass (green dots, total). Dots represent experimental points ± SD, and lines correspond to Gompertz modeling done on the 20 first days of culture ± 95% uncertainty ($R^2_{N\ total}$=0.99; $R^2_{N\ pelagic}$=0.98; $R^2_{[Chla]\ total}$=0.99; $R^2_{[Chla]\ pelagic}$=0.97). The arrows indicate the entrance in the stationary and senescent phases, respectively.

cells^{-1}, and then finally decrease to 2.0 ± 0.1 µg 10^6 cells^{-1} at the end of the culture (Fig. 4**,** online resource **Table S2**). This progressive decrease was observed for both $Chl_{a\ spe}$ and $CarT_{spe}$ (Fig. 4**,** online resource **Table S2**), with $Chl_{a\ spe}$ decreasing more rapidly as a significant increase in CarT/Chl_a was observed from 0.53 ± 0.00 µg 10^6 cells^{-1} in the exponential growth phase to 0.62 ± 0.02 µg 10^6 cells^{-1} at the end of the culture.

The pelagic cells had a lower specific pigment content on average, compared to the mean cellular pigment content in the total biomass, however they showed a comparable decrease in total cell pigment content (online resource **Table S2**). At the

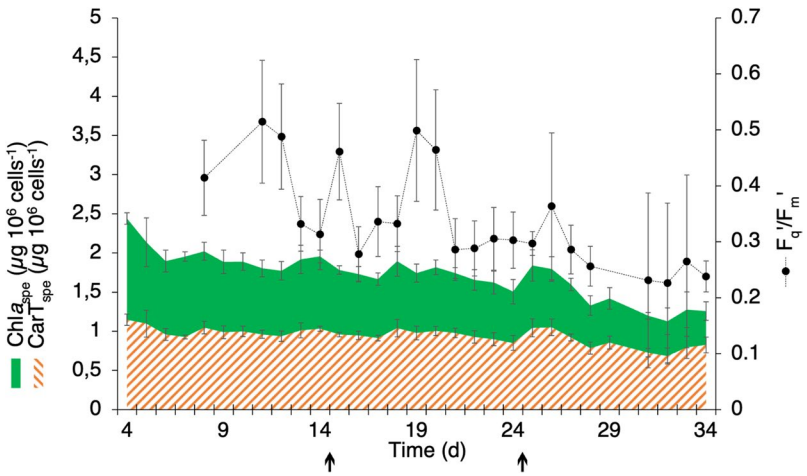

Fig. 4 Physiological profile of *H. ostrearia* cells during its cultivation in MPBR. Physiological parameters are $Chl_{a\ spe}$, the specific Chl_a content of cells of the total biomass (plain green area, µg 10^6 cells^{-1}), $CarT_{spe}$, the specific total carotenoid content of cells in the total biomass (lined orange area, µg 10^6 cells^{-1}). All values are presented as mean ± SD of n = 3. The last physiological parameter is F_q'/F_m', effective quantum yield of PSII at growth irradiance measured for pelagic biomass (for PAR = 200 µmol photons m^{-2} s^{-1}) (plain black dots, arbitrary units). Values were estimated from the daily measured P/E curve ± SE. The arrows indicate the entrance in the stationary and senescent phases, respectively.

pigment composition level, differences were sharpened, and significant changes were observed before the end of the culture. From the late stationary phase, there was a significant decrease in pelagic cell specific Chl_a content from 1.5±0.1 µg 10^6 cells^{-1} to 1.3±0.1 µg 10^6 cells^{-1}, whereas pelagic cell specific CarT content significantly increased from 0.9 ±0.1 µg 10^6 cells^{-1} to 1.0 ±0.1 µg 10^6 cells^{-1} (online resource **Table S2**). The balance between $CarT_{spe}$ and $Chl_{a\ spe}$ of the pelagic biomass shifted significantly by the second half of the stationary phase, occurring earlier than it did in the total biomass sample.

As a complementary indicator of the physiological state of the biomass, the evolution of the effective photosynthetic capacity F_q'/F_m' of the resuspended cells was monitored (Fig. 4). A great variability between two consecutive days was observed, yet two distinct patterns were identified, one before and one after day 20. Before day 20, the effective photosynthetic yield F_q'/F_m' at growth irradiance (*i.e.* 200 µmol photons m^{-2} s^{-1}), appeared to be highly variable from one day to the next, with a mean value of 0.40 ± 0.09 (a.u.). After day 20, a small but regular decrease in F_q'/F_m' was observed, reaching 0.28 ± 0.04 (a.u.), indicating a progressive degradation of the algal photosynthetic apparatus from the second half of the stationary phase.

Blue water quality

Polydispersity distribution

For 34 days, the supernatant of culture was harvested daily by filtration at a rate of 100 mL day^{-1} and the samples were separated in three lots named BW1, BW2 and BW3, corresponding to the three growth stages of the population described above, exponential, stationary, and senescent stage, respectively. Interestingly, when 75% and 74% of EMn were recovered in the concentrated BW2 and BW3, respectively, only 33% was recovered during the filtration on 3-kDa membrane for BW1. These differences in retention behavior prevented the recovery of the same EMn quantities for BW1, as illustrated by the concentration factor (Table 1).

Spectral analysis

To evaluate possible changes in EMn extract composition between lots, a sample of each lot was analyzed by ATR-FTIR (Fig. 5a). As the standard refining technique used in this study does not yield a fully purified EMn extract, the spectra likely reflect a mixture of compounds rather than EMn alone (as proposed by Latigui et al. (2024)). In particular, several characteristic EPS-related bands (online resource **Table S3**) often observed in microalgae EPS (Bélanger et al. 2020; Borjas Esqueda et al. 2022; Sanniyasi et al. 2022) were identified in these spectra. All three extracts displayed characteristic polysaccharide bands, with the broad band around 3300 cm^{-1} corresponding to O-H stretching, associated with the band observed around 1100 cm^{-1} and 1040 cm^{-1} assigned to C-O-C and C-C liaisons of the pyranose stretching, respectively. BW1 displayed some dissimilarities, with some peaks standing out compared to BW2 and BW3 spectra, particularly one around 2924 cm^{-1}, associated with the CH_2 stretching, and another at 858 cm $^{-1}$ associated to a glycosidic linkage in the polymer. The band at 1424 cm^{-1}, associated to COO- stretching, also discriminated BW1, being relatively higher in that lot. Eventually, the lower relative absorbance of the band around 1547 cm^{-1}, associated with amide II group stretching, and the higher relative absorbance of the one at 1100 cm^{-1}, associated to pyran rings vibrations, appeared to differentiate the most BW1 from both BW2 and BW3.

In the UV-Visible spectrum (Fig. 5b), no significant difference was observed. All three lots had a maximal absorbance in the 660 nm region, corresponding to the absorbance of the chromophore. The characteristic band around 230 nm was observed, and no difference in the 230/660 absorbance ratio was noticed from one BW lot and another. The absence of a distinct absorbance band around 322 nm, characteristic of the purified EMn (Pouvreau et al. 2006a), is not surprising considering the low selectivity enabled by double ultrafiltration, which results in incomplete purification.

Table 1 Preconcentration ultrafiltration of the culture supernatant, over a 3 kDa membrane, using an AMICON cell (P = 1.5 bar, stirring = 250 rpm). VRF, volumetric reduction factor during ultrafiltration of BW, CF_{EMn}, concentration factor of EMn according to the absorbance at 669 nm of the solution

Lots	Harvesting stage	VRF	CF_{EMn}	Initial BW		Concentrated BW	
				pH	Salinity (ppt)	pH	Salinity (ppt)
BW1	Exponential	13	4	7.4	29	7.7	29
BW2	Stationary	11	9	7.6	30	7.7	30
BW3	Senescent	11	8	7.5	30	7.5	31

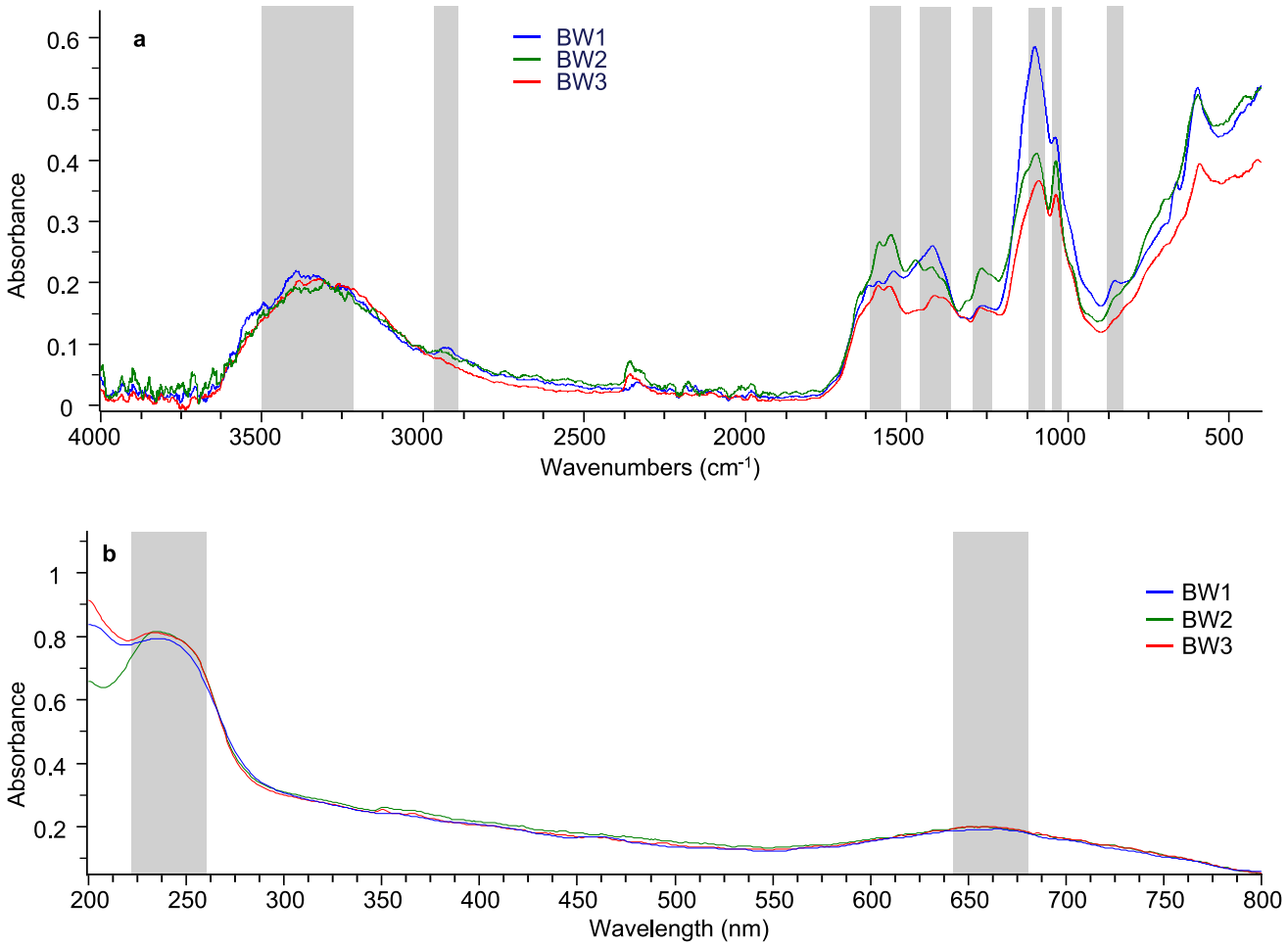

Fig. 5 Absorption spectra of the marennine extracts produced by *H. ostrearia,* harvested during exponential, stationary and senescent phase of its culture in MPBR (D=0.1 day^{-1}). (**a**) ATR-FTIR and (**b**) UV-Visible spectrum of marennine extracts BW1, BW2 and BW3.

Blue Water bioactivities

BW1 displayed a significantly higher potency to inhibit the development of *V. splendidus* 4D1-8, with 20% growth inhibition at 5.5 ± 0.3 mg L^{-1} of EMn (Fig. 6a). BW2 and BW3 displayed a halved efficiency, reaching 20% bacterial growth inhibition at 11.9 ± 0.6 and 15.5 ± 0.4 mg L^{-1} of EMn respectively (F (2,6) = 18.312, p =0.003, online resource **Table S4**).

Regarding DPPH scavenging ability, no difference was observed between the three BW lots (Fig. 6b). The harvest time of the lots alone or in interaction with [EMn] did not induce significant differences to the linear dose-response curve (BW1, p = 0.556; BW2, p = 0.714; [EMn]*BW1, p = 0.482; [EMn]*BW2, p = 0.771, online resource **Table S5**) and the EMn concentration was the only significant factor of the scavenging response (R^2 =0.97, [EMn], t(2) = 6.106, p = 0.009, online resource **Table S5**). As illustrated in **Fig.** 6b**, 20**% of the DPPH radicals were scavenged when the EMn concentration reached 19 ± 3 mg L^{-1} of EMn, regardless of the harvesting period.

Discussion

The purpose of this study was to assess the extent to which marennine production varies through time when *H. ostrearia* is cultivated in a MPBR, and standard methods are applied for both its refining and quantification. The key findings indicated that over the 34 days of culture, both the extracellular marennine (EMn) productivity and the extract's bioactivities changed in relation to the growth phases of the cultivated biomass.

Under MPBR culture conditions, three distinct phases were observed in *H. ostrearia* cultures: an exponential phase until day 15, a stationary phase from day 15 to day 25, and a senescent phase thereafter. The onset of the stationary

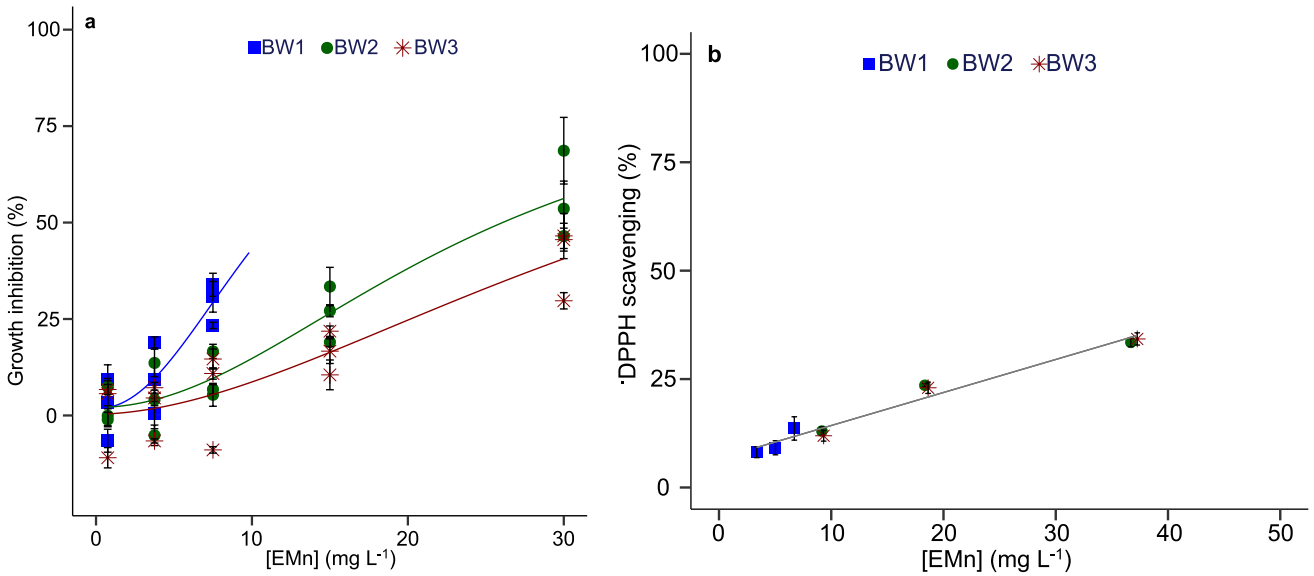

Fig. 6 Bioactivity of marennine extracts harvested at three distinct stages of *H. ostrearia* NCC531 MPBR culture. (**a**) Dose-response curves of *V. splendidus* 4D1-8 exposed to a marennine concentration range [EMn] (mg L^{-1}) over 24 h exposition. Each value represents the mean ± SD (n = 3), and three clones of the *Vibrio* strain were exposed to each extract. $R^2_{exponential}$ = 0.77, $R^2_{stationary}$ = 0.90, R^2_{end} = 0.79. (**b**) Dose-response curve of DPPH radicals scavenging exposed to a marennine concentration range [EMn] (mg L^{-1}). R2=0,97. Each value represents the mean ± SD (n = 3). BW1 in blue (square), BW2 in green (circle), and BW3 in red (cross).

phase was marked by stabilization of biomass concentration. Around day 20, visible changes of cells physiological states were observed in chlorophyll *a* fluorescence, with a low plateau in PSII effective quantum yield. In parallel, a shift in pigment composition occurred, with increased relative carotenoid content and decreased total pigment concentration, consistent with a decline in photosynthetic capacity and stress-induced biomass degradation (Li et al. 2021; Adjout et al. 2022). From day 25 onward, total and pelagic biomass declined together with pigment content, confirming the onset of senescence. Thus, changes in physiological states of *H. ostrearia* cells were confirmed over 34 days of culture in MPBR.

These physiological shifts were also reflected in EMn production. During exponential growth, cells reached their maximum specific productivity (maximum R_{cell} = 12.4 ± 1.7 mg 10^6 $cells^{-1}$ day^{-1} of EMn), which decreased during the stationary phase and ceased in senescence. By day 15, EMn concentration in the culture medium reached 21.2 ± 0.7 mg L^{-1} of EMn (online resource **Fig**. S1), a level previously reported to slow down *H. ostrearia* growth due to shading (Pouvreau et al. 2007). This blue pigment accumulation changing the light environment, together with increased carotenoid proportion, potentially reflect photoacclimation processes (Brunet et al. 2011). However, in diatoms under low-light conditions – to which shading would be associated – chlorophyll *a* content typically increases relative to carotenoids to sustain photosynthesis (Li et al. 2021), which was not observed here. Alternative or additional factors likely contributed to the observed evolution of cells physiological state. Phosphorus availability in the MPBR, although not completely depleted (Online Resource, **Table S6**), remain the limiting nutrient in the MPBR culture conditions (Nghiem Xuan et al. 2021; Gargouch et al. 2022). Furthermore, the perfusion mode, with only 10% daily renewal of supernatant, could have led to accumulation of extracellular polymeric substances (EPS) and cell lysates, contributing to stress and oxidative damage as reported in diatoms exposed to reactive oxygen species (ROS) accumulation (Li et al. 2021). Together, these environment conditions modifications could explain the decrease in pigment content, rise in carotenoid proportion, and growth arrest reflecting the progressive physiological deterioration of *H. ostrearia* in MPBR.

Altogether, our results highlight a progressive metabolic shift in *H. ostrearia* cells within the MPBR. These changes, driven by culture conditions, likely modified the composition of the culture supernatant, notably through alterations in EPS production. Diatoms are well known for producing a wide range of EPS, whose metabolism is strongly dependent on their physiological state (Underwood et al. 2004). While *H. ostrearia* has mainly been studied for EMn production, it also synthesizes other EPS (Bélanger et al. 2025). The fluctuations observed in EMn productivity may therefore represent only the visible component of a broader metabolic shift of EPS production, for which patterns remain unknown in *H. ostrearia*. In addition, the progressive accumulation of cell lysates in the MPBR is expected to further alter the culture supernatant. Together, these processes likely affect

not only EMn yield but also the overall quality of the extract obtained through standard ultrafiltration procedure. The EMn extracts collected along the three main phases of the *H. ostrearia* culture, exponential (BW1), stationary (BW2), and senescent (BW3) exhibited some differences concerning both bioassays and spectral analyses.

Results from the bioassays indicated that EMn extract quality evolved over the course of *H. ostrearia* culture, but not all bioactivities were equally affected. BW1 showed the most effective inhibition of bacterial growth ($IC20_{BW1} = 5.5 \pm 0.3$ mg L^{-1} of EMn) compared to BW2 and BW3. By contrast, antioxidant activity (DPPH scavenging) remained consistent across all three BW lots ($IC20 = 19 \pm 3$ mg L^{-1} of EMn), and its variability was mainly explained by EMn concentration measured via the standard spectrophotometry method.

Spectral analyses indicate compositional differences among the extracts beyond the EMn chromophore. The latter, according to the UV-vis spectra, remained stable throughout the three EMn extracts. Given that EMn has a retention time of 10 days in the MPBR culture supernatant, this stability is consistent with the observations reported by Prasetiya et al. (2022), who confirmed EMn chromophore stability up to 20 days under comparable conditions (light and temperature) using standard spectrophotometry. Meanwhile, ATR-FTIR profiles revealed more pronounced EPS-associated bands in BW1, with a more pronounced carbohydrate-related bands (C–O–C vibration at 1100 $cm^{-}1$) (Tseng et al. 1996; Borjas Esqueda et al. 2022), whereas BW2 and BW3 exhibited stronger absorption near 1547 $cm^{-}1$, typically associated with amide groups (Borjas Esqueda et al. 2022). Since no amide groups have been reported in EMn structure (Yusuf et al. 2023; Zebiri et al. 2023), this feature is likely related to co-extracted compounds such as cell lysates accumulating during the later phases of culture. Compared to purified EMn spectra reported by Latigui et al. (2024) our extracts exhibited similar hydroxyl and glycosidic signatures but lacked clear quinone- and carbonyl-specific signals, likely due to relative amount of co-extracted compounds. Such observations are consistent with refining results: BW1 (exponential phase) displayed lower retention on a 3-kDa cut-off membrane than BW2 and BW3, indicating an apparent increase in molecular weight over culture time, the presence of various substituent groups and monomeric units within the macromolecules, or association with other macromolecules in later culture stages. Altogether spectral analysis suggests the accumulation of other metabolites along the culture in the supernatant coextracted and thus modifying the quality of the EMn extract obtain through standard procedure.

The preserved antioxidant activity aligns with the stability of the chromophore, consistent with previous studies identifying this moiety as the main determinant of radical scavenging activity (Pouvreau et al. 2008; Prasetiya et al. 2021). Spectrophotometric quantification of EMn, based on chromophore absorptivity, therefore provides a good proxy for antioxidant efficiency but does not inform on the heteropolysaccharide moiety recently described (Yusuf et al. 2023; Zebiri et al. 2023). In contrast, the decline in antibacterial efficiency suggests additional structural or compositional changes of the EMn extract. Two non-exclusive hypotheses can be proposed: (i) modifications of the EMn polysaccharide backbone, potentially reducing accessibility or functionality of active sites; (ii) accumulation of co-extracted metabolites (other EPS, cellular debris) during culture, which could mask or compete with antibacterial sites, acting as inhibitors.

These findings indicate that functional groups responsible for antioxidant and antibacterial properties likely differ, and their relative abundance may vary with culture progression. The chromophore appears resilient, whereas the polysaccharide moiety—or its interactions with co-produced EPS—seems more vulnerable to changes occurring over time. Further research should focus on marennine's structural variability and its associations with other EPS. Combining enzymatic assays with advanced structural analyses could help clarify the molecular determinants of each bioactivity and the impact of co-extracted compounds.

Conclusion

This study demonstrates that EMn extract quality varies during *Haslea ostrearia* culture in a MPBR, a system that decouples biomass and supernatant residence times. While EMn chromophore stability preserved antioxidant activity, antibacterial efficiency declined, likely due to compositional changes or co-extracted compounds. These findings underscore the need to standardize production parameters such as culture stage at harvest, dilution rate of the culture, and refining protocols to ensure consistent extract quality.

The molecular complexity of EMn extract, particularly its polysaccharide moiety and interactions with other extracellular polymeric substances, has significant implications for its biotechnological applications, including antibacterial agents. We hypothesize that EMn structural variability is driven by changes in its polysaccharide moiety and associations with co-produced EPS during culture. Future research should combine advanced structural analyses (e.g., NMR, mass spectrometry, and enzymatic profiling) with bioactivities assays to clarify these mechanisms and guide strategies for optimized EMn production.

Supplementary Information The online version contains supplementary material available at https://doi.org/10.1007/s10811-025-03690-y.

Authors' contributions **Conceptualization**: Elodie Pedron, Réjean Tremblay, Jean-Sébastien Deschênes, Olivier Gonçalves, Anthony Massé; **Methodology**: Elodie Pedron, Marylise Duperthuy, Réjean Tremblay, Jean-Sébastien Deschênes, Olivier Gonçalves, Anthony Massé; **Formal analysis and investigation**: Elodie Pedron, Jean-Luc Mouget, Marylise Duperthuy, Annabelle Mathieu-Denoncourt, Céline Laroche, Réjean Tremblay, Jean-Sébastien Deschênes, Olivier Gonçalves, Anthony Massé; **Writing - original draft preparation**: Elodie Pedron; **Writing - review and editing**: Elodie Pedron, Jean-Luc Mouget, Marylise Duperthuy, Annabelle Mathieu-Denoncourt, Céline Laroche, Réjean Tremblay, Jean-Sébastien Deschênes, Olivier Gonçalves, Anthony Massé; **Funding acquisition**: Jean-Luc Mouget, Réjean Tremblay, Jean-Sébastien Deschênes, Olivier Gonçalves, Anthony Massé; **Resources**: Marylise Duperthuy, Céline Laroche, Réjean Tremblay, Jean-Sébastien. Deschênes, Olivier Gonçalves, Anthony Massé; **Supervision**: Marylise Duperthuy, Réjean Tremblay, Jean-Sébastien Deschênes, Olivier Gonçalves, Anthony Massé.

Funding This work is part of a project that has received funding from the European Union's Horizon 2020 research and innovation program under grant agreement N° 734708/GHaNA/H2020-MSCA-RISE-2016 (J.-L.M.) and was supported by the Ressources Aquatiques Québec (RAQ) Research Network supported by the Fonds de Recherche du Québec-Nature et Technologies N° 2014-RS-171172. This work also received funding from the Institut France-Québec pour la coopération scientifique en appui au secteur maritime (IFQM) and Nantes Université for E.P.'s PhD position.

Data availability Data will be made available on request.

Declarations

Competing Interests The authors declare that they have no known competing financial interests or personal relationships that could have influenced the work reported in this study.

References

Adjout R, Mouget J, Pruvost J, Chentir I, Loiseau C, Baba Hamed MB (2022) Effects of temperature, irradiance, and pH on the growth and biochemical composition of *Haslea ostrearia* batch-cultured in an airlift plan-photobioreactor. Appl Microbiol Biotechnol 106:5233–5247

Bachtiar E, Lestari AD, Astuty S, Sunarto S, Prasetiya FS (2024) Effect of extracellular marennine produced by *Haslea ostrearia* on the blood clams *Tegillarca granos*a. J Aquac Fish Health 13:102–109

Bélanger W, Arnold AA, Turcotte F, Saint-Louis R, Deschênes J-S, Genard B, Marcotte I, Tremblay R (2020) Extraction improvement of the bioactive blue-green pigment "marennine" from diatom *Haslea ostrearia*'s blue water: a solid-phase method based on graphitic matrices. Mar Drugs 18:653

Bélanger W, Saint-Louis R, Genard B, Deschênes J-S, Tremblay R (2025) Scalable purification of marennine and other exopolymers from diatom *Haslea ostrearia*'s "blue water." Algal Res 86:103879

Bergé J-P, Bourgougnon N, Alban S, Pojer F, Billaudel S, Chermann J-C, Robert JM, Franz G (1999) Antiviral and anticoagulant activities of a water-soluble fraction of the marine diatom *Haslea ostrearia*. Planta Med 65:604–609

Borjas Esqueda A, Gardarin C, Laroche C (2022) Exploring the diversity of red microalgae for exopolysaccharide production. Mar Drugs 20:246

Bouhlel Z, Arnold AA, Deschênes J-S, Mouget J-L, Warschawski DE, Tremblay R, Marcotte I (2021) Investigating the action of the microalgal pigment marennine on *Vibrio splendidus* by *in vivo* ^{2}H and ^{31}P solid-state NMR. Biochim Biophys Acta Biomembr 1863:183642

Brunet C, Johnsen G, Lavaud J, Roy S (2011) Pigments and photoacclimation processes. In: Roy S, llewellyn CA, Egeland ES, Johnsen G (eds) Phytoplankton Pigments: Characterization, Chemotaxonomy and Applications in Oceanography. Cambridge University Press, Cambridge, pp 445-471

Chehouri M, Pedron E, Genard B, Doiron K, Fortin S, Bélanger W, Deschênes J-S, Tremblay R (2025) "Bleu VS Yellow": Marennine and extracellular polysaccharides for potential application in cosmetic and pharmaceutical applications. The Microbe 8:100448

Consalvey M, Perkins RG, Paterson DM, Underwood GJC (2005) PAM fluorescence: a beginners guide for benthic diatomists. Diatom Res 20:1–22

De Brouwer JFC, Stal LJ (2002) Daily fluctuations of exopolymers in cultures of the benthic diatoms *Cylindrotheca closterium* and *Nitzschia* sp. (Bacillariophyceae). J Phycol 38:464–472

Falaise C, Cormier P, Tremblay R, Audet C, Deschênes J-S, Turcotte F, François C, Seger A, Hallegraeff G, Lindquist N, Sirjacobs D, Gobert S, Lejeune P, Demoulin V, Mouget J-L (2019) Harmful or harmless: biological effects of marennine on marine organisms. Aquat Toxicol 209:13–25

Falaise C, James A, Travers M-A, Zanella M, Badawi M, Mouget J-L (2019) Complex relationships between the blue pigment marennine and marine bacteria of the genus *Vibrio*. Mar Drugs 17:160

Gang Y, Eom T-Y, Marasinghe SD, Lee Y, Jo E, Oh C (2021) Optimising the DPPH assay for cell-free marine microorganism supernatants. Mar Drugs 19:256

Gargouch N, Touchard R, Marec H, Luc Mouget J, Pruvost J, Massé A (2022) Submerged membrane photobioreactor for the cultivation of *Haslea ostrearia* and the continuous extraction of extracellular marennine. Bioresour Technol 350:126922

Gastineau R, Turcotte F, Pouvreau J-B, Morançais M, Fleurence J, Windarto E, Prasetiya FS, Arsad S, Jaouen P, Babin M, Coiffard L, Couteau C, Bardeau J-F, Jacquette B, Leignel V, Hardivillier Y, Marcotte I, Bourgougnon N, Tremblay R, Deschênes J-S, Badawy H, Pasetto P, Davidovich NA, Hansen G, Dittmer J, Mouget J-L (2014) Marennine, promising blue pigments from a widespread *Haslea* diatom species complex. Mar Drugs 12:3161–3189

Laroche C (2022) Exopolysaccharides from microalgae and cyanobacteria: diversity of strains, production strategies, and applications. Mar Drugs 20:336

Latigui A, Jacquette B, Dittmer J, Bardeau J-F, Boivin E, Beaulieu L, Pasetto P, Mouget J-L (2024) Spectral properties of marennine-like pigments reveal minor differences between blue *Haslea* species and strains. Molecules 29:5248

Li Z, Li W, Zhang Y, Hu Y, Sheward R, Irwin AJ, Finkel ZV (2021) Dynamic photophysiological stress response of a model diatom to ten environmental stresses. J Phycol 57:484–495

Martinho De Brito M, Bundeleva I, Marin F, Vennin E, Wilmotte A, Plasseraud L, Visscher PT (2023) Properties of exopolymeric substances (EPSs) produced during cyanobacterial growth: potential role in whiting events. Biogeosciences 20:3165–3183

Myklestad S, Holm-Hansen O, Vårum KM, Volcani BE (1989) Rate of release of extracellular amino acids and carbohydrates from the marine diatom *Chaetoceros affinis*. J Plankton Res 11:763–773

Nghiem Xuan R, Mouget JL, Turpin V, Jaouen P, Pruvost J (2021) Optimization of the growth and marennine production by the diatom *Haslea ostrearia* in photobioreactor. Algal Res 55:102251

Nghiem-Xuan R (2019) Optimisation de la culture d'*Haslea ostrearia* en photobioréacteur. These de doctorat, Nantes

Oyanedel D, Labreuche Y, Bruto M, Amraoui H, Robino E, Haffner P, Rubio T, Charrière GM, Le Roux F, Destoumieux-Garzón D (2020) *Vibrio splendidus* O-antigen structure: a trade-off between virulence to oysters and resistance to grazers. Environ Microbiol 22:4264–4278

Pedron E, Gargouch N, Mouget J-L, Tremblay R, Deschênes J-S, Massé A, Gonçalves O (2023) Hybrid photobioreactor operation for the intensified production of *Haslea ostrearia* and marennine in function of strain variability. Algal Res 75:103285

Permatasari I, Prasetiya FS, Arsad S, Agung MUK, Mouget J-L (2019) Antibacterial activity of *Haslea ostrearia* supernatant adapted in Indonesia against pathogenic bacteria relevant to mariculture (*in-vitro* study). Omni-Akuatika 15:30–38

Pouvreau J-B (2006) Purification et caractérisation du pigment bleu-vert "marennine" synthétisé par la diatomée marine *Haslea ostrearia* (Gaillon/Bory) Simonsen : propriétés physico-chimiques et activités biologiques. These de doctorat, Nantes

Pouvreau J-B, Housson E, Tallec LL, Morançais M, Rincé Y, Fleurence J, Pondaven P (2007) Growth inhibition of several marine diatom species induced by the shading effect and allelopathic activity of marennine, a blue-green polyphenolic pigment of the diatom *Haslea ostrearia* (Gaillon/Bory) Simonsen. J Exp Mar Biol Ecol 352:212–225

Pouvreau J-B, Morançais Michèle, Taran F, Rosa P, Dufossé Laurent, Guérard Fabienne, Pin S, Fleurence J, Pondaven P (2008) Antioxidant and free radical scavenging properties of marennine, a blue-green polyphenolic pigment from the diatom *Haslea ostrearia* (Gaillon/Bory) Simonsen responsible for the natural greening of cultured oysters. J Agric Food Chem 56:6278–6286

Pouvreau J-B, Morançais M, Fleury F, Rosa P, Thion L, Cahingt B, Zal F, Fleurence J, Pondaven P (2006) Preliminary characterisation of the blue-green pigment "marennine" from the marine tychopelagic diatom *Haslea ostrearia* (Gaillon/Bory) Simonsen. J Appl Phycol 18:757–767

Pouvreau J-B, Morançais M, Massé G, Rosa P, Robert J-M, Fleurence J, Pondaven P (2006) Purification of the blue-green pigment "marennine" from the marine tychopelagic diatom *Haslea ostrearia* (Gaillon/Bory) Simonsen. J Appl Phycol 18:769–781

Prasetiya FS, Foret M, Deschênes J-S, Gastineau R, Mouget J-L, Tremblay R (2022) Semi-continuous system for benthic diatom cultivation and marennine production. Algal Res 62:102633

Prasetiya FS, Ramdhani DS, Mulyani Y, Agung MUK, Arsad S, Mouget J-L (2021) Antioxidant activities of culture supernatant *Haslea ostrearia* adapted in Indonesia. AACL Bioflux 14:9

Prasetiya FS, Safitri I, Widowati I, Cognie B, Decottignies P, Gastineau R, Morançais M, Windarto E, Tremblay R, Mouget J-L (2016) Does allelopathy affect co-culturing *Haslea ostrearia* with other microalgae relevant to aquaculture? J Appl Phycol 28:2241–2254

Provasoli L, McLaughlin JJA, Droop MR (1957) The development of artificial media for marine algae. Arch Mikrobiol 25:392–428

Ritchie RJ (2008) Universal chlorophyll equations for estimating chlorophylls *a, b, c*, and *d* and total chlorophylls in natural assemblages of photosynthetic organisms using acetone, methanol, or ethanol solvents. Photosynthetica 46:115–126

Rossignol N, Lebeau T, Jaouen P, Robert JM (2000) Comparison of two membrane–photobioreactors, with free or immobilized cells, for the production of pigments by a marine diatom. Bioproc Biosyst Eng 23:495–501

Sanniyasi E, Patrick APR, Rajagopalan K, Gopal RK, Damodharan R (2022) Characterization and in vitro anticancer potential of exopolysaccharide extracted from a freshwater diatom *Nitzschia palea* (Kütz.) W.Sm. 1856. Sci Rep 12:22114

Shimamura T, Sumikura Y, Yamazaki T, Tada A, Kashiwagi T, Ishikawa H, Matsui T, Sugimoto N, Akiyama H, Ukeda H (2014) Applicability of the DPPH assay for evaluating the antioxidant capacity of food additives – inter-laboratory evaluation study –. Anal Sci 30:717–721

Shnyukova EI, Zolotariova YK (2015) Diatom exopolysaccharides: a review. Int J Algae 17:50–67

Strickland JDH, Parsons TR (1968) A practical handbook of seawater analysis. Fish Res Bd Canada Bull 167:185–194

Tardy-Laporte C, Arnold AA, Genard B, Gastineau R, Morançais M, Mouget J-L, Tremblay R, Marcotte I (2013) A ^{2}H solid-state NMR study of the effect of antimicrobial agents on intact *Escherichia coli* without mutating. Biochim Biophys Acta 1828:614–622

Tseng DY, Vir R, Traina SJ, Chalmers JJ (1996) A Fourier-transform infrared spectroscopic analysis of organic matter degradation in a bench-scale solid substrate fermentation (composting) system. Biotechnol Bioeng 52:661–671

Turcotte F, Mouget J-L, Genard B, Lemarchand K, Deschênes J-S, Tremblay R (2016) Prophylactic effect of *Haslea ostrearia* culture supernatant containing the pigment marennine to stabilize bivalve hatchery production. Aquat Living Resour 29:401

Turpin V, Robert J-M, Goulletquer P (1999) Limiting nutrients of oyster pond seawaters in the Marennes-Oléron region for *Haslea ostrearia*: applications to the mass production of the diatom in mesocosm experiments. Aquat Living Resour 12:335–342

Turpin V, Robert J-M, Goulletquer P, Massé G, Rosa P (2001) Oyster greening by outdoor mass culture of the diatom *Haslea ostrearia* Simonsen in enriched seawater. Aquacult Res 32:801–809

Underwood GJC, Boulcott M, Raines CA, Waldron K (2004) Environmental effects on exopolymer production by marine benthic diatoms: dynamics, changes in composition, and pathways of production. J Phycol 40:293–304

Yusuf M, Baroroh U, Nuwarda RF, Prasetiya FS, Ishmayana S, Novianti MT, Tohari TR, Hardianto A, Subroto T, Mouget J-L, Pasetto P (2023) Theoretical and experimental studies on the evidence of 1,3-β-glucan in marennine of *Haslea ostrearia*. Molecules 28:5625

Zebiri I, Jacquette B, Francezon N, Herbaut M, Latigui A, Bricaud S, Tremblay R, Pasetto P, Mouget J-L, Dittmer J (2023) The polysaccharidic nature of the skeleton of marennine as determined by NMR spectroscopy. Mar Drugs 21:42